Development of chitosan/montmorillonite nanocomposites with encapsulated α-tocopherol

Marali Vilela Dias [a,*], Viviane Machado Azevedo [a], Soraia Vilela Borges [a], Nilda de Fátima Ferreira Soares [b], Regiane Victória de Barros Fernandes [c], João José Marques [d], Éber Antonio Alves Medeiros [b]

[a] Food Science Department, Federal University of Lavras, 37200-000 Lavras, MG, Brazil
[b] Food Technology Department, Federal University of Viçosa, 36570-000 Viçosa, MG, Brazil
[c] Institute of Agricultural Sciences, Campus de Rio Paranaíba, Federal University of Viçosa, 38810-000 Rio Paranaíba, MG, Brazil
[d] Soil Science Department, Federal University of Lavras, 37200-000 Lavras, MG, Brazil

ARTICLE INFO

ABSTRACT

Nanocomposites of chitosan (CS) were developed and characterized in a full factorial design with varying levels of montmorillonite (MMTNa) and encapsulated tocopherol (toc-encap). The structural properties (XRD, FTIR), morphology (TEM), hygroscopic properties (water vapour permeability, hydrophobicity, sorption isotherms) and optical properties (haze, CIELab parameters) of the resulting materials were evaluated. Toc-encap contents up to 10% influenced the intercalation of MMTNa in the CS matrix, resulting in films with reduced water vapour permeability (3.48×10^{-11} (g/m s Pa)), increased hydrophobicity ($\Delta G_{Hydroph}$ |7.93–59.54| mJ m^{-2}) and lower equilibrium moisture content (EMC), thus showing potential for active food packaging materials. At levels above 10%, toc-encap agglomerates occurred, which deteriorated the properties of the resulting films, as shown with the TEM. As the toc-encap content increased, the films became slightly more yellow, more irregular and less transparent, with a higher haze index.

© 2014 Elsevier Ltd. All rights reserved.

1. Introduction

Chitosan is the second-most abundant natural polysaccharide and is non-toxic, biodegradable, and able to form films with antimicrobial properties (Leceta, Guerrero, & de la Caba, 2013). Chitosan films exhibit high permeability to water vapour due to its hydrophilic nature (Sanchez-Gonzalez, Chafer, Chiralt, & Gonzalez-Martinez, 2010), which limits its application in food. The introduction of nanoscale particles, such as montmorillonite clay (MMT), can improve the mechanical and barrier properties of biodegradable films, as previously reported (Dias et al., 2013; Lavorgna, Piscitelli, Mangiacapra, & Buonocore, 2010; Silvestre, Duraccio, & Cimmino, 2011; Wang et al., 2005).

MMT clay is a natural silicate material with a layered structure and a wide variety of potential applications, including as adsorbents, filters, catalysts, agents for the preparation of charged polymer nanocomposites and materials for the encapsulation of functional substances, molecules and organisms (Ennajih, Bouhfid, Essassi, Bousmina, & El Kadib, 2012; Sothornvit, Hong, An, & Rhim, 2010). The silicate layers in MMT tend to be organised

into stacks that are held together by van der Waals forces. To obtain polymers with improved characteristics, it is necessary to break the attractive forces between the layers, thus allowing the polymer to penetrate the clay structure. Consequently, the distance between the layers will increase, forming an intercalated or exfoliated structure. Exfoliation or delamination maximises the polymer/clay interactions, resulting in more significant changes in the physical properties of the material (Pavlidou & Papaspyrides, 2008).

It is highly possible that clay layers interleaved with chitosan molecules lead to polar interactions between the negatively charged silicate layers and the polycationic polymer (Ennajih et al., 2012; Lavorgna et al., 2010; Pandey & Mishra, 2011).

Along with the use of biodegradable packaging, the production of healthy and natural foods may be achieved by the use of functional packages, which have an active function to enrich food. Addition of nutrients in the package, with the goal of migration of substances for the food has the advantage of avoiding the loss of nutrients due to the processing steps (heat treatment) to which foods are subjected. After food processing, it will be enriched in the packaging containing functional substances, such as vitamins, minerals or amino acids.

α-Tocopherol (vitamin E) is synthesized only by photosynthetic organisms. It is interesting to incorporate this vitamin in packages aimed at fortifying foods. However, the applications of α-tocopherol are limited due to its highly hydrophobic nature and sensitivity to oxygen, heat and light (Liang et al., 2012). Encapsulation of active components, such as tocopherol, may be one alternative that can preserve their function, control diffusion and ensure their effectiveness as vitamins for consumers (Malheiros, Daroit, da Silveira, & Brandelli, 2010), and can represent a functional and enriched approach to food packaging.

This study reports the development of chitosan/MMTNa films with encapsulated α-tocopherol and the evaluation of their morphological, structural, barrier and optical properties which are important for initial characterization of packaging intended for food.

2. Materials and methods

2.1. Materials

Chitosan (CS) was supplied by Polymar Ciência e Nutrição S/A, Fortaleza, Brazil, (PM = 71.3 kDa) with a deacetylation degree of 85.9%. Glacial acetic acid was purchased from Sigma–Aldrich (São Paulo, Brazil). Encapsulated DL-α-tocopherol acetate (toc-encap) (50% DL-α-tocopherol, 24.5% maltodextrin, 24.5% starch and 10% silicon dioxide) and natural sodium montmorillonite clay (MMTNa) were supplied by DSM Nutritional Products Ltda (São Paulo, Brazil) and Southern Clay Products, Inc. (Texas, EUA), respectively.

2.2. Experimental design

A full factorial design with the following factors was used: 0% and 1% for MMTNa, and 0%, 5%, 10% and 20% for toc-encap. The experiment was conducted using a completely randomized design with 3 replications.

2.3. Preparation of chitosan nanocomposite films

CS films were prepared according to the method of Zhong, Song, and Li (2011), with some modifications to obtain flexible and homogeneous films. A filmogenic solution of CS (Film 1) was prepared by dissolving 2.0 g of CS powder in 100 ml of aqueous acetic acid solution (0.5% v/v). This mixture was allowed to stand for two hours to ensure hydration of the polysaccharide. To ensure complete dissolution, the solution was subjected to stirring (1000 rpm) for 6 h using a magnetic stirrer at room temperature (24 °C). The filmogenic solution was filtered with filter paper and a vacuum pump to remove non-solubilised CS. The pH of the filmogenic solution was adjusted to 4.9 with acetic acid to avoid any MMTNa structural changes and to ensure protonation of the amino groups in the CS structure ($-NH_3^+$) (Pandey & Mishra, 2011). This filmogenic solution was used for all films.

The MMTNa nanoparticles were used at a concentration of 1% (p/p). CS with 1% MMTNa (Film 2), was prepared by heating the filmogenic solution to 40 °C and then adding the nanoparticles. The filmogenic solution was stirred for 30 min with a magnetic stirrer at 40 °C and then subjected to ultrasonic homogenisation (Sonifier Cell Disruptor Branson – Model 450D, Manchester, UK), for 36 min at 80 W. The glass transition temperature for CS is 40 °C (dos Santos, da PSoares, Dockal, Filho, & Cavalheiro, 2003). At this temperature, the polymer chains exhibited greater movement, facilitating the incorporation of MMTNa into chitosan molecules.

Toc-encap was added to the filmogenic CS solution (Film 1) at concentrations of 5%, 10% and 20%, and stirred for 30 min with a magnetic stirrer at room temperature. These suspensions were homogenised with an Ultra-Turrax homogeniser (T 25, Ika-Werke, Germany) for 5 cycles, each lasting 2 min at 15,000 rpm. Lastly, the solutions were subjected to ultrasonic homogenisation (36 min/80 W), yielding Films 3, 4 and 5 (with 5%, 10%, and 20% toc-encap, respectively).

For Films 6, 7 and 8, solutions of toc-encap (5%, 10% or 20% p/p toc-encap/QUI) and MMTNa (1.0% p/p MMTNa/QUI) were prepared. The solutions were stirred for 30 min with a magnetic stirrer at room temperature and subjected to ultrasonic homogenisation for 45 min/80 W to facilitate the intercalation of the toc-encap molecules into the clay lamellae. Subsequently, solutions of toc-encap and MMTNa in a filmogenic solution of CS (Film 1) were heated separately up to 40 °C and then poured into one another. Lastly, solutions were magnetically stirred, homogenised with an Ultra-Turrax homogeniser and then with an ultrasonic homogeniser as described for Films 3, 4 and 5. For film formation, 145 ml of the solutions were cast onto glass plates (608 cm^2) and dried at 25 °C for 24 h to ensure slow evaporation of the solvent. All films were kept at a controlled temperature of 23 ± 2 ° C and a relative humidity of 50 ± 5% RH for 48 h before analysis by the method (ASTM, 2000a).

2.4. Film characterisation

2.4.1. X-ray diffraction (XRD)

The crystalline structure of the chitosan polymer and the morphology of the MMTNa clay in the polymer were determined by a Philips model PW1840 diffractometer (35 kV and 25 mA) equipped with cobalt radiation (CoKα, λ = 1.725 Å). The scattering angles ranged from 2° to 35° at a scanning rate of 0.02°/min.

2.4.2. Transmission electron microscopy (TEM)

The morphologies of the particles in the filmogenic solution containing toc-encap were observed by transmission electron microscopy (TEM) (Zeiss EM 109) at a voltage of 80 kV. A drop of the film solution was placed on a copper grid (400 mesh), and the excess liquid was removed with filter paper. The grid was air dried and then uranyl acetate (2%) was added for contrast (Azeredo et al., 2010). Based on the results obtained for the various filmogenic solutions, a film containing toc-encap and MMTNa was selected for the clay dispersion visualisation.

The dispersion of the clay nanocomposites selected was visualised by TEM (Tecnai G2-12 – Spiritbiotwin Fei) at a voltage of 120 kV. Films with a width of 1 mm were placed in *Eppendorf* tubes and gradually infiltrated at 24 °C using a Spurr resin/ethanol gradient (30% resin for 8 h, 70% resin for 12 h and three cycles of 100% resin for 24 h each). After infiltration, the films were mounted in the mold and cured in an oven at 65 °C for 24 h. Cross-sections with a thickness of 60 nm were obtained using an ultramicrotome with a diamond knife and placed directly onto copper grids.

2.4.3. Water vapour permeability (WVP)

Water vapour permeability (WVP) tests were carried out according to ASTM (2000c) with some modifications. The film was sealed in a permeation cell containing anhydrous calcium chloride. The permeation cell was placed in a humidity chamber with a controlled temperature, at 23 ± 2 °C, and maintained at 75% relative humidity (RH). The water vapour permeability was determined, based on the mass of water absorbed by the permeation cell, considering the RH difference between both environments (outside and inside the cell). The samples were weighed to a constant weight, and the weight gain values were plotted as a function of time. The slope of each line was calculated by

performing a linear regression ($R^2 > 0.9$), and the water vapour transmission rate (WVTR, g/h/m^2) was calculated as the slope of the line divided by the area of exposed film (m^2). The WVP (g/(m s Pa)) was calculated by the following equation:

$$WVP = \frac{WVTR}{\Delta P} \cdot x \tag{1}$$

where x is the film thickness and ΔP is the saturation vapour pressure of water (Pa) between the faces of the film: $\Delta P = S(R_1 - R_2)$; S is the saturation vapour pressure at the experimental temperature (2809 kPa); R_1 is the RH outside of the capsule (75%); and R_2 is the RH within the capsule containing calcium chloride (0%).

2.4.4. Surface hydrophobicity

The surface hydrophobicity of the films was estimated using the optical contact angle method using a goniometer (Krüss$^®$, Germany) equipped with image analysis software. Drops (2 μl) of milli-Q water, formamide (Sigma–Aldrich – São Paulo, Brazil) and α-bromonaphthalene (Sigma–Aldrich – São Paulo, Brazil) were deposited on the film, and the contact angles (°) were measured. To interpret the surface free energy as a function of the intermolecular forces at the interface and determine the free energy of hydrophobicity ($\Delta G_{\text{Hydroph}}$), several authors have already used the Van Oss approach, also known as the Lifshitz-van der Waals/acid–base approach (Araújo, Bernardes, Andrade, Fernandes, & Sá, 2009; Bialopiotrowicz, 2003; Camilloto et al., 2010). According to this approach, Young's equation is determined by the contact angle (θ) measured for at least three different liquids (two of which are polar). This equation expresses the contact angle formed by a liquid on a solid surface:

$$(1 + \cos\theta)\gamma_1 = 2\left(\sqrt{\gamma_s^{LW}\gamma_l^{LW}} + \sqrt{\gamma_s^+\gamma_l^-} + \sqrt{\gamma_s^-\gamma_l^+}\right) \tag{2}$$

where γ_l is the surface tension of the liquid; γ^{LW} is the polar component or the Lifshitz-van der Waals component, which contains contributions from dispersion, induction and orientation interactions with the surface (γ_s) or liquid (γ_l); γ^+ is the electron acceptor parameter of the polar component of the surface tension; and γ^- is the electron donor parameter of the polar component of the surface tension (s) or liquid (l) (Araújo et al., 2009). The free energy of hydrophobic interaction ($\Delta G_{\text{Hydroph}}$) is expressed according to Van Oss (1995):

$$\Delta G_{\text{Hydroph}} = \Delta G_{sws}^{LW} + \Delta G_{sws}^{AB} \tag{3}$$

where ΔG_{sws}^{LW} is the adhesive nonpolar interaction energy (Lifshitz-Van der Waals) between the surface and water:

$$\Delta G_{sws}^{LW} = -2\left(\sqrt{\gamma_s^{LW}} - \sqrt{\gamma_w^{LW}}\right)^2 \tag{4}$$

and ΔG_{SWS}^{AB} is expressed in terms of the cohesive polar energy interaction between the acceptor electrons and the donor electron surface ($\sqrt{\gamma_s^+\gamma_s^-}$), the polar cohesive energy of interaction between the acceptor electrons and donor electrons of water molecules ($\sqrt{\gamma_w^+\gamma_w^-}$), the polar energy of adhesive interaction between the surface acceptor electrons and donor electrons of water molecules ($\sqrt{\gamma_s^+\gamma_w^-}$), and the polar energy of adhesive interaction between the surface donor electrons and acceptor electrons of water ($\sqrt{\gamma_w^+\gamma_s^-}$):

$$\Delta G_{sws}^{AB} = -4\left(\sqrt{\gamma_s^+\gamma_s^-} + \sqrt{\gamma_w^+\gamma_w^-} - \sqrt{\gamma_s^+\gamma_w^-} - \sqrt{\gamma_w^+\gamma_s^-}\right) \tag{5}$$

2.4.5. Moisture sorption (MS)

The moisture sorption was determined according to the method described by Pereda, Amica, and Marcovich (2012). The films (1.8 × 1.8 cm) were dried at 40 °C for three days (50 ± 5 mmHg)

in a vacuum oven, and placed inside a desiccator maintained at 75% relative humidity (RH) and 23 ± 1 °C to determine the kinetics of water sorption. The samples were weighed at regular time intervals with a precision of ±0.0001 g. The curves were fitted according to the Fick equation for one-dimensional diffusion of a solute in a flat plane (Cranck, 1975):

$$\frac{M_t}{M_\infty} = 1 - \frac{8}{\pi^2}\sum_{n=0}^{\infty}\frac{1}{(2n+1)^2}\exp\left[-\left(\frac{(2n+1)^2\pi^2Dt}{\delta^2}\right)\right] \tag{6}$$

where M_t is the moisture content of the sample at a fixed time expressed on the dry basis [%], M_∞ is the amount of water absorbed at equilibrium, D is the effective diffusion coefficient, t is the time and δ is the average thickness of the film. This equation is valid in the specific case of mass transport through a planar sheet with constant boundary conditions and uniform initial moisture distribution, and the edge effects can be neglected. The equilibrium moisture content (EMC) of the films at 75% relative humidity (RH) was also calculated.

2.4.6. Fourier transform infrared spectra (FT-IR)

FT-IR spectra were collect using a spectrophotometer equipped with a KBr-DTGS detector and a KBr beam splitter (FTIR-Thermo Scientific Nicolet 6700, USA). The spectra were obtained at a resolution of 4 cm^{-1} in the range of 4000 to 400 cm^{-1}, with 56 scans per spectrum.

2.4.7. Optical properties

The optical properties of the films were determined using a Color Quest XE colourimeter (Hunter Associates Laboratory, Inc., Reston, VA, USA). Colour CIELab parameters were obtained using D$_{65}$ illumination and observation at 10° in reflectance mode. The following parameters were measured: haze index, lightness (L^*), intensity of yellow/blue (b^*) and saturation index (c^*). The transparency of the films was determined by measuring the percent transmittance (%T) at 600 nm using a spectrophotometer (GBC UV/VIS 918, Shimadzu, Japan) as reported by Sothornvit et al. (2010). The transparency (T_{600}) was calculated using the following equation:

$$T_{600} = \text{Log}\%T/\delta \tag{7}$$

where δ is the film thickness (mm).

2.4.8. Statistical analysis

WVP, MS, $\Delta G_{\text{Hydroph}}$ and the optical properties were analysed using Statistica software (ver. 8, Stat Soft Inc., Tulsa, USA). The analysis of variance (ANOVA) test was used to evaluate the significance of the differences between factors and levels. The FT-IR, XRD and TEM results were analysed descriptively.

3. Results and discussion

3.1. General

All films were translucent, flexible, homogeneous and apparently free of pores or cracks. Films 5 and 8 were brittle.

3.2. XRD analysis of CS/MMTNa/toc-encap nanocomposites

The CS film (Film 1) exhibited no crystalline peaks, indicating the formation of an amorphous structure (Fig. 1). The absence of crystallinity in the CS film was attributed to the presence of residual acetic acid solvent. This may hinder the formation of inter- and intramolecular hydrogen bonds in CS, resulting in a less organised structure (Wang et al., 2005). According to Wang et al. (2005), the dried CS films still contain a small amount of acetic acid in the form
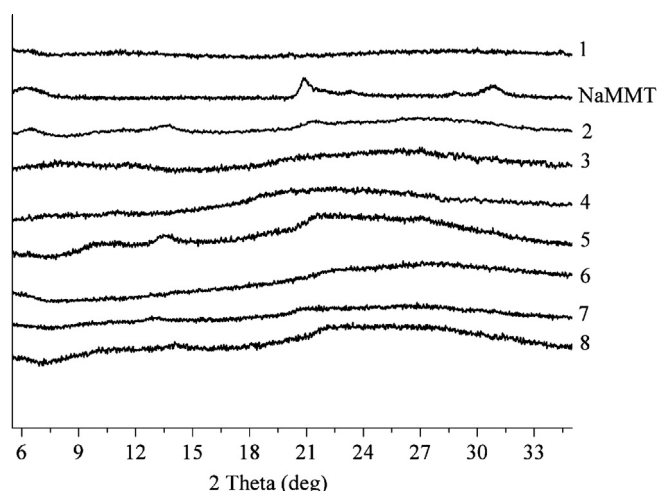
Fig. 1. XRD patterns of chitosan/ montmorillonite (MMTNa)/encapsulated tocopherol nanocomposites. Films: (1) CS; (2) CS/MMTNa; (3) CS/5toc-encap; (4) CS/ 10toc-encap; (5) CS/20toc-encap; (6) CS/MMTNa/5toc-encap; (7) CS/MMTNa/ 10toc-encap; (8) CS/MMTNa/20toc-encap.

of chitosan acetate. Lavorgna et al. (2010) observed characteristic peaks indicating crystallinity and a broad peak corresponding to an amorphous structure for CS films. The crystal structure of CS is strongly dependent on the treatment, processing, origin and molecular constitution, such as the degree of deacetylation and molecular weight (Srinivasa, Ramesh, & Tharanathan, 2007).

The diffractogram of the MMTNa clay exhibited a characteristic diffraction peak at $2\theta = 8.09°$ and $22.9°$, corresponding to the spacing between the individual MMT layers of $d = 12.7$ and 4.51 Å, respectively. The CS structure was altered by the addition of MMTNa and toc-encap. The CS is susceptible to structural changes due to the large amount of reactive groups, such as hydroxyl and amino groups (dos Santos et al., 2003).

After the incorporation of the MMTNa into CS (Film 2), the diffraction peaks shifted to $6.35°$ and $21.4°$ (i.e., a spacing of $d = 16.2$ and 4.82 Å), corresponding to an expansion of the clay layers. This showed that the CS macromolecules are able to intercalate into the MMTNa layers. The incorporation of MMTNa clay into CS gave rise to another crystalline region around $2\theta = 13.7°$ (spacing $d = 7.52$ Å). Film 2 may have developed a flocculated structure that can be attributed to edge-edge hydrogen bonding interactions between the hydroxyl groups present on the edges of the layered silicate (Lavorgna et al., 2010). The movement of the basal reflection of MMTNa to lower angles indicates the formation of an intercalated nanostructure, while the peak broadening indicates a disordered intercalated or exfoliated structure (Wang et al., 2005). Film 3 (5% toc-encap) exhibited an amorphous structure. Film 4 (10% toc-encap) exhibited a peak around $20.6°$ and more crystallinity due to the high concentration of toc-encap, with peaks at $13.3°$, $9.73°$ and a large peak at $21.4°$. This indicated that the starch used to encapsulate the tocopherol altered the film structure, forming ordered and crystalline regions. According to other authors, starch exhibits a crystalline structure with peaks around 15, 17 and 23°. Maltodextrin is characterised by an amorphous structure (Bai & Shi, 2011; Waliszewski, Aparicio, Bello, & Monroy, 2003).

Film 6 (5% toc-encap/MMTNa) exhibited an enlarged peak at $21.8°$ with a spacing of $d = 4.74$ Å. This may have indicated the exfoliation of MMTNa due to its low concentration and the good interactions between MMTNa and toc-encap. According to Tunc and Duman (2010), MMTNa has hydrophilic characteristics and disperses well in water. In the process used to produce these films, the MMTNa was treated with an ultrasonic homogeniser with

toc-encap and water. This treatment may have improved the dispersion of the clays.

Film 7 (10% toc-encap/MMTNa) exhibited peaks at $12.8°$ and $20.6°$ with spacings of $d = 8.00$ and 5.00 Å, respectively, and these values are higher than those of Film 2.

Film 8 (20% toc-encap/ MMTNa) exhibited an enlarged peak at $21.8°$ ($d = 4.74$ Å) and another peak between $9.51°$ and $13.7°$. This indicated that MMTNa and toc-encap interacted well with one another. According to Zhong et al. (2011), the existence of a large amorphous peak indicates that the intermolecular interactions between the components restricting the movement of the polymer chains prevents crystallisation. In the presence of toc-encap, the MMTNa binds to starch, increasing the interlayer distance due to the intercalation of the clay.

3.3. Transmission electron microscopy analysis (TEM)

TEM analysis was used to confirm the degree of intercalation or exfoliation of the clay. Micrographs a, b and c (Fig. 2) represent the filmogenic solutions of films 3, 4 and 5, respectively (12,000×). The micrographs show the toc-encap particles dispersed in the filmogenic solution. The solution with 20% toc-encap (Fig. 2c) exhibited agglomeration, while the 10% solution exhibited a smaller toc-encap particle size (Fig. 2b), resulting in a more homogeneous film with potentially improved properties. The filmogenic solution with 5% toc-encap exhibited large, well-distributed particles (Fig. 2a).

The MMT clay dispersion in Film 2 exhibited exfoliated and intercalated structures (Fig. 2d, 98,000×). Film 7 (CS/10toc-encap/MMTNa) exhibited essentially exfoliated structures and a few intercalated structures (Fig. 2e and f, respectively). In nanocomposite materials, an exfoliated structure is more preferable than an intercalated structure (Tunc & Duman, 2010). Comparing Films 2 and 7, Film 7 prepared with toc-encap exhibited a higher percentage of exfoliated structures. This observation is consistent with the results of the XRD analysis.
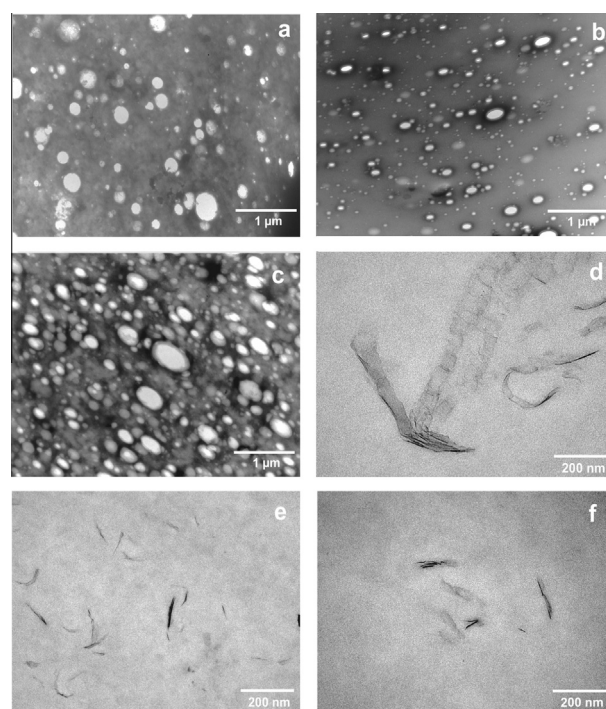
Fig. 2. TEM micrographs of filmogenic solutions and chitosan nanocomposites: (a) CS/5toc-encap; (b) CS/10toc-encap; (c) CS/20toc-encap; (d) CS/MMTNa; (e and f) CS/MMTNa/10toc-encap.

3.4. Fourier-transform infrared spectroscopy (FT-IR)

FT-IR analysis was performed to determine the characteristics of the polymer matrix as well as the changes in the intermolecular interactions among the nanocomposites (Zhong et al., 2011). When the compounds are blended, chemical interactions and physical links reflect changes in spectral peaks (Martins, Cerqueira, & Vicente, 2012). Fig. 3 shows the FT-IR spectrum of CS/MMT/toc-encap.

All of the films, except for 2, 5 and 7, exhibited a broad band in the region of 3700–3000 cm^{-1} attributed to the stretching vibration of the –OH group (Li, Guo, Lin, Fan, & Song, 2010; Martinez-Camacho et al., 2010; Martins et al., 2012). Film 2 did not show this peak because the –OH groups of CS are attached to MMTNa. Film 5, with 20% toc-encap, exhibited a high concentration of agglomerated encapsulant (starch and maltodextrin), with the result that the –OH groups were not detected in this film. Film 7 (10% toc-encap/MMTNa) had –OH groups attached to the clay, with no peak in the region characteristic of the –OH group.

The absorption band at 2924 cm^{-1} was assigned to the C—H stretching vibration (Li et al., 2010; Tripathi, Mehrotra, & Dutta, 2010). The FT-IR spectra clearly showed a peak at 1560 cm^{-1}, corresponding to the vibration of the protonated amino group with acetic acid, chitosan acetate (–NH$_3^+$Ac$^-$) (Wang et al., 2005). The presence of –NH^{+3}Ac$^-$ is responsible for the amorphous structure of the CS film, which was confirmed by XRD analysis. The peak at 1750 cm^{-1}, characteristic of the presence of a carbonyl group (C=O) (Martins et al., 2012), appeared in Films 4, 5, 7 and 8, containing 10% to 20% toc-encap. The main absorption band characteristic of the CS films appeared at 1631 cm^{-1}, attributed to the combination of C–O stretching (amide I) and –NH bending. The peak at 1405 cm^{-1}, characteristic of –CN, (Li et al., 2010) appeared in all the films.

In the region of the band between 1200–1300 cm^{-1}, a new peak appeared at 1245 cm^{-1} when toc-encap was added, which can be related to the vibration of the –OH groups of starch and maltodextrin (Martins et al., 2012).

3.5. Water vapour permeability (WVP)

A significant difference was observed between the WVP values of the films prepared with or without MMTNa ($p < 0.05$) (Table 1).

The inclusion of MMTNa decreased the WVP of the film. This fact was interesting for application in foods with higher water
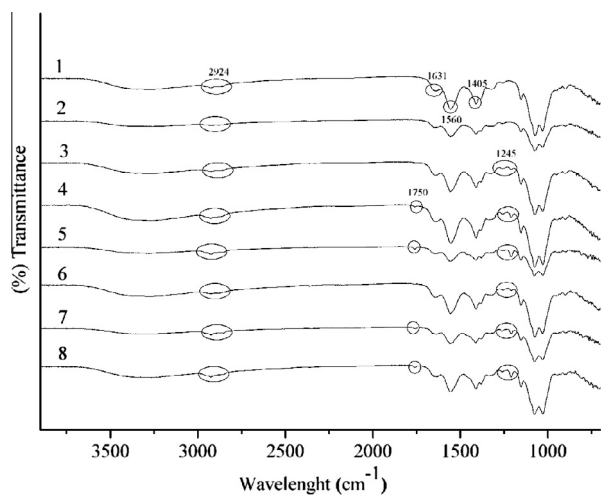
Table 1
Values of water vapour permeability (WVP).

Films	WVP × 10^{11} (g/m s Pa)
With MMTNa	3.48 ± 0.25[b]
Without MMTNa	4.49 ± 1.00[a]

MMTNa = Natural sodium montmorillonite clay.

* Means observed in the column with the same letter do not differ statistically ($p < 0.05$).

activities. The process of water vapour transport simultaneously depends on the solubility and diffusion of water in the polymer matrix (Zhong et al., 2011). MMTNa reduced the water solubility by binding to the hydroxyl groups (–OH) of the CS and the starch and maltodextrin used to encapsulate tocopherol. The diffusion of water was also reduced by the increase in the tortuosity of its route through the polymer matrix. The inclusion of nanoparticles in films lengthens the permeant path through the polymeric matrix, thus reducing the diffusivity and making the film a stronger barrier to water vapour. CS molecules penetrate into the interlayer space by increasing the distance between the layers, thus increasing the tortuosity of the path through the MMTNa.

Other researchers have reported similar WVP values for CS films. Lavorgna et al. (2010) found values of 2.38 and 2.14 g/m s Pa × 10^{-11} (ΔRH 50%, 25 °C) for CS films and CS films with 3% MMTNa, respectively. Moreover, Sanchez-Gonzalez et al. (2010) reported a value of 124 g Pa^{-1} s^{-1} m^{-1} × 10^{-11} for a CS film at ΔRH 50%, 20 °C. This variation could be the source of the differences in the degree of deacetylation, molecular weight and other characteristics among CS films.

3.6. Surface hydrophobicity

When the free energy of the hydrophobic interaction ($\Delta G_{Hydroph}$) is less than zero, the free energy of interaction between molecules is attractive and the affinity for water molecules is less than the intermolecular affinity, indicating that a material is hydrophobic. If the opposite is true ($\Delta G_{Hydroph} > 0$), then the film is hydrophilic (Camilloto et al., 2010).

For the analysis of variance (ANOVA), the interactions between the factors MMTNa and tocopherol were significant for $\Delta G_{Hydroph}$, and adjusted models are presented in Table 2.

Fig. 4 shows that the addition of toc-encap decreased the hydrophobicity of the films without MMTNa and exerted a variable effect on the films containing MMTNa. For the films without MMTNa, the film without toc-encap exhibited exhibited the greater |$\Delta G_{Hydroph}$|, indicating a greater hydrophobicity. CS requires an acidic solution to protonate the NH^{2+} groups and enable dissolution in water. However, in the absence of acid, CS molecules have a higher

Table 2
Adjusted equations for the free energy of hydrophobic interaction ($\Delta G_{Hydroph}$, mJ m^{-2}), colour parameters (b^*, C^*, L^*), transparency (%), haze index (%), equilibrium moisture content (EMC), and diffusion coefficient (D, mm^2/min × 10^{-7}).

Analysis	Films	
	With MMTNa	Without MMTNa
$\Delta G_{Hydroph}$	$-15.3-11.6x+0.57x^2$ ($R^2 = 0.80$)	$-60.4+2.04x$ ($R^2 = 0.82$)
b^*	$10.5+0.34x$ ($R^2 = 0.74$)	$12.9+0.15x$ ($R^2 = 0.65$)
c^*	$10.6+0.33x$ ($R^2 = 0.74$)	$12.9+0.15x$ ($R^2 = 0.65$)
L^*	$90.1-0.19x$ ($R^2 = 0.84$)	$88.9-0.1x$ ($R^2 = 0.83$)
Analysis	*All films*	
Transparency	$42.9-0.96 \times$ ($R^2 = 0.96$)	
Haze index	$55.4+0.72x-0.03x^2$ ($R^2 = 0.50$)	
EMC	$22.2-0.49x$ ($R^2 = 0.84$)	
D	$17.2+1.53x$ ($R^2 = 0.53$)	

x: concentration of toc-encap.

Fig. 3. FT-IR spectra of CS nanocomposites. (1) CS; (2) CS/MMTNa; (3) CS/5toc-encap; (4) CS/10toc-encap; (5) CS/20toc-encap; (6) CS/MMTNa/5toc-encap; (7) CS/MMTNa/10toc-encap; (8) CS/MMTNa/20toc-encap.
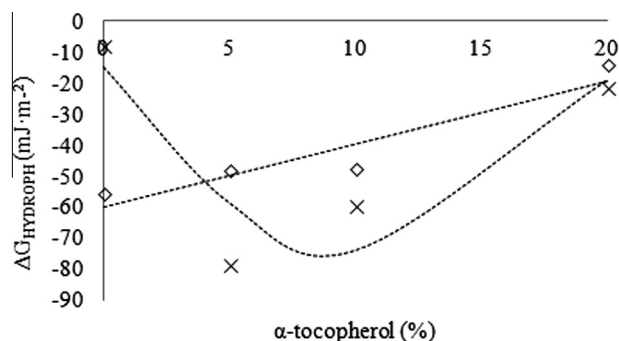
Fig. 4. Free energy of hydrophobic interaction of chitosan nanocomposites as a function of toc-encap concentration. Films without MMTNa (◇) and with MMTNa (×). The dashed lines represent the adjusted values.

affinity for one another than for the molecules of water. The addition of toc-encap decreased $\Delta G_{Hydroph}$, indicating an increase in hydrophilicity. This is due to the destruction of the crystalline structure of the starch molecule used as an encapsulant, which was pre-gelatinised by the acetic acid present in the formulation during the heating of the film solution, resulting in free hydroxyl groups and a consequent increase in hygroscopicity (Bourtoom & Chinnan, 2008; Pelissari et al., 2012). The greater hydrophobicity of the CS film compared with the starch film was reported by Bangyekan, Aht-Ong, and Srikulkit (2006).

For the films containing both MMTNa and toc-encap, the two components interacted ($p < 0.05$). The interaction between starch and MMTNa (hydrogen bond) reduced the availability of the hydrophilic groups, thus decreasing the hydrophilicity (Lavorgna et al., 2010; Pelissari et al., 2012).

This interaction increased the distance between the clay layers, increasing the hydrophobicity of the film as the toc-encap concentration increased. This was observed for concentrations up to 10%. Above this amount of toc-encap, the attraction between the molecules of the encapsulating tocopherol, starch and maltodextrin prevails, leading to the agglomeration of these particles as seen in the TEM micrographs. Therefore, above 10% of toc-encap, there is less interaction between the starch and MMTNa, increasing the hydrophilicity of the film, which is not suitable for food preservation.

According to Su et al. (2010), the contact angle with water is a good indicator of the degree of hydrophilicity of the films. Lower contact angles with water imply a greater hydrophilicity. Angles greater than 50° indicate a hydrophobic surface (Araújo et al., 2009). Leceta et al. (2013) measured a contact angle with water of 105° for CS films, indicating that these films are hydrophobic.

3.7. Moisture sorption

According to Zhong et al. (2011), the water content in the CS films increases with increasing water activity. Furthermore, the increases are slow at low water activity, and increase considerably at water activities above 0.75. The toc-encap significantly affected ($p < 0.05$) the moisture balance (EMC) and diffusion coefficient (D). Table 2 shows the equations for these responses.

At 75% relative humidity, hydration and swelling of the hydrophilic groups of CS and encapsulants (starch and maltodextrin) occur. Under these conditions, the polymer chains are swollen, and a reduced number of sites are available to absorb water. As the toc-encap content increased, the degree of swelling increased, decreasing the amount of space available for water molecules, and hence decreasing the EMC of the film.

Hydration occurs because CS has a strong affinity for water, and in solid form, the macromolecules may have twisted structures that are easily hydrated (dos Santos et al., 2003).

In contrast, diffusion involves the transport of the permeant through non-crystalline regions, and is enhanced by the movement of polymer chains, creating voids (Sarantópoulos et al., 2002). Increasing toc-encap increased the crystallinity of the film structures. The water adsorbed by the polymer chains during swelling broke the intermolecular interactions and crystal structure, increasing the mobility of the polymer chains and the speed of transmission of water. Therefore, greater amounts of toc-encap lead to greater swelling and chain movement, and increases in the number of molecules diffusing through the polymer and in the diffusion coefficient.

3.8. Optical properties

The optical properties are essential for the applications of these films (Pereda et al., 2012). Certain foods allow transparent packaging for visualization of the product by the consumer, while others require protection from light.

The amount of tocopherol had significant effects on the transparency and haze index. The level of transparency is related to the internal film structure (Sanchez-Gonzalez et al., 2010). Higher concentrations of toc-encap increased the crystallinity of the films, preventing the transmission of light through the film, i.e., reducing the transparency of the film. Therefore, films with toc-encap are more opaque than CS films (Table 2).

Montmorillonite layers have a thicknesses less than the wavelength of visible light, and therefore do not divert light and are transparent (de Oliveira Faria, Vercelheze, & Mali, 2012).

In transmission mode, the light scattered by a sample is responsible for the reduced ability to visualise objects through the film and is measured by the haze index. The scattering of light as it passes through a layer or film can yield a hazy or smoky field when objects are viewed through the material (ASTM, 2000b).

The haze index is related to the surface irregularities and heterogeneity, and is influenced by specific parameters involved in film formation, such as the degree of dispersion, the type of clay, component compatibility and particle size (Sothornvit et al., 2010). The inclusion of toc-encap increased the haze index of these films. This indicates that in addition to increasing the crystallinity of the films, toc-encap increases the irregularity of the film surface. In general, these films exhibited haze indexes much larger than that of polypropylene films, which is 25% according to Asuka, Kouzai, Liu, Minoru, and Nitta (2006).

The interactions among parameters L^*, b^* and c^* were significant ($p < 0.05$). Films with and without MMTNa exhibited the same behaviours with respect to these parameters. Chroma (c^*), a measure of colour saturation (Zhong et al., 2011) and the b^* value (yellow staining) increased for all films with the concentration of toc-encap. However, films without MMTNa exhibited a less pronounced increase in the values of c^* and b^* when compared with films containing MMTNa. Sothornvit et al. (2010) reported an increase in the b^* value due to the use of MMTNa in whey protein isolate films. The increase in toc-encap reduced the L^* value for all films. Films with MMTNa were lighter than the films without clay.

4. Conclusions

The toc-encap did not affect the water vapour permeability, exhibited good intercalation of MMTNa, resulting in films with a more hydrophobic surface and a lower EMC, thus showing potential for active food packaging materials.

Acknowledgements

References

Araújo, E. A., Bernardes, P. C., Andrade, N., Fernandes, P. É., & Sá, J. (2009). Hidrofobicidade de ribotipos de *Bacillus cereus* isolados de indústria de laticínios. *Alimentos e Nutrição Araraquara, 20*(3), 491–498.

ASTM, (2000a). Standard practice for conditioning plastics for testing, D618-00. In Standard practice for conditioning plastics for testing, (p. 4). Philadelphia, PA.

ASTM, (2000b). Standard test method for haze and luminous transmittance of transparent plastics, D1003-00. In, (p. 6). Philadelphia, PA.

ASTM, (2000c). Standard test method for water vapor transmission of materials, E96-00. In, (p. 9). Philadelphia, PA.

Asuka, K., Kouzai, I., Liu, B. P., Minoru, T., & Nitta, K. H. (2006). Effects of Silica Particles on the Transparency of Polypropylene Based Nanocomposites. In T. Shiono, K. Nomura & M. Terano (Eds.), Progress in Olefin Polymerization Catalysts and Polyolefin Materials, Proceedings of the First Asian Polyolefin Workshop, vol. 161 (pp. 237–240).

Azeredo, H. M. C., Mattoso, L. H. C., Avena-Bustillos, R. J., Ceotto, G., Munford, M. L., Wood, D., et al. (2010). Nanocellulose reinforced chitosan composite films as affected by nanofiller loading and plasticizer content. *Journal of Food Science, 75*(1), N1–N7.

Bai, Y., & Shi, Y. C. (2011). Structure and preparation of octenyl succinic esters of granular starch, microporous starch and soluble maltodextrin. *Carbohydrate Polymers, 83*(2), 520–527.

Bangyekan, C., Aht-Ong, D., & Srikulkit, K. (2006). Preparation and properties evaluation of chitosan-coated cassava starch films. *Carbohydrate Polymers, 63*(1), 61–71.

Bialopiotrowicz, T. (2003). Wettability of starch gel films. *Food Hydrocolloids, 17*(2), 141–147.

Bourtoom, T., & Chinnan, M. S. (2008). Preparation and properties of rice starch-chitosan blend biodegradable film. *LWT–Food Science and Technology, 41*(9), 1633–1641.

Camilloto, G. P., Pires, A. C. S., Soares, N. D. F., Araujo, E. A., Andrade, N. J., & Ferreira, S. O. (2010). Effect of active packaging incorporated with triclosan on bacteria adhesion. *Journal of Food Science, 75*(8), E557–E564.

Cranck, J. (1975). *The mathematics of diffusion*. Oxford: Clarendon. 71.

de Oliveira Faria, F., Vercelheze, A. E. S., & Mali, S. (2012). Propriedades físicas de filmes biodegradáveis à base de amido de mandioca, álcool polivinílico e montmorilonita. *Quimica Nova, 35*(3), 487–492.

Dias, M. V., Soares, N. D. F., Borges, S. V., de Sousa, M. M., Nunes, C. A., de Oliveira, I. R. N., et al. (2013). Use of allyl isothiocyanate and carbon nanotubes in an antimicrobial film to package shredded, cooked chicken meat. *Food Chemistry, 141*(3), 3160–3166.

dos Santos, J. E., da PSoares, J., Dockal, E. R., Filho, S. P. C., & Cavalheiro, É. T. (2003). Caracterização de quitosanas comerciais de diferentes origens. *Polímeros Ciência e Tecnologia, 13*(4), 242–249.

Ennajih, H., Bouhfid, R., Essassi, E. M., Bousmina, M., & El Kadib, A. (2012). Chitosan-montmorillonite bio-based aerogel hybrid microspheres. *Microporous and Mesoporous Materials, 152*, 208–213.

Lavorgna, M., Piscitelli, F., Mangiacapra, P., & Buonocore, G. G. (2010). Study of the combined effect of both clay and glycerol plasticizer on the properties of chitosan films. *Carbohydrate Polymers, 82*(2), 291–298.

Leceta, I., Guerrero, P., & de la Caba, K. (2013). Functional properties of chitosan-based films. *Carbohydrate Polymers, 93*(1), 339–346.

Li, Y. Y., Guo, X. L., Lin, P. F., Fan, C. C., & Song, Y. H. (2010). Preparation and functional properties of blend films of gliadins and chitosan. *Carbohydrate Polymers, 81*(2), 484–490.

Liang, N., Sun, S., Li, X., Piao, H., Piao, H., Cui, F., et al. (2012). α-Tocopherol succinate-modified chitosan as a micellar delivery system for paclitaxel: Preparation, characterization and in vitro/in vivo evaluations. *International Journal of Pharmaceutics, 423*(2), 480–488.

Malheiros, P. D., Daroit, D. J., da Silveira, N. P., & Brandelli, A. (2010). Effect of nanovesicle-encapsulated nisin on growth of *Listeria monocytogenes* in milk. *Food Microbiology, 27*(1), 175–178.

Martinez-Camacho, A. P., Cortez-Rocha, M. O., Ezquerra-Brauer, J. M., Graciano-Verdugo, A. Z., Rodriguez-Felix, F., Castillo-Ortega, M. M., et al. (2010). Chitosan composite films: Thermal, structural, mechanical and antifungal properties. *Carbohydrate Polymers, 82*(2), 305–315.

Martins, J. T., Cerqueira, M. A., & Vicente, A. A. (2012). Influence of α-tocopherol on physicochemical properties of chitosan-based films. *Food Hydrocolloids, 27*(1), 220–227.

Pandey, S., & Mishra, S. B. (2011). Organic-inorganic hybrid of chitosan/organoclay bionanocomposites for hexavalent chromium uptake. *Journal of Colloid and Interface Science, 361*(2), 509–520.

Pavlidou, S., & Papaspyrides, C. D. (2008). A review on polymer-layered silicate nanocomposites. *Progress in Polymer Science, 33*(12), 1119–1198.

Pelissari, F. M., Yamashita, F., Garcia, M. A., Martino, M. N., Zaritzky, N. E., & Grossmann, M. V. E. (2012). Constrained mixture design applied to the development of cassava starch-chitosan blown films. *Journal of Food Engineering, 108*(2), 262–267.

Pereda, M., Amica, G., & Marcovich, N. E. (2012). Development and characterization of edible chitosan/olive oil emulsion films. *Carbohydrate Polymers, 87*(2), 1318–1325.

Sanchez-Gonzalez, L., Chafer, M., Chiralt, A., & Gonzalez-Martinez, C. (2010). Physical properties of edible chitosan films containing bergamot essential oil and their inhibitory action on *Penicillium italicum*. *Carbohydrate Polymers, 82*(2), 277–283.

Sarantópoulos, C. I., de Oliveira, L. M., Padula, M., Coltro, L., Alves, R. M. V., & Garcia, E. E. C. (2002). Embalagens plásticas flexíveis: principais polímeros e avaliação de propriedades: CETEA/ITAL.

Silvestre, C., Duraccio, D., & Cimmino, S. (2011). Food packaging based on polymer nanomaterials. *Progress in Polymer Science, 36*(12), 1766–1782.

Sothornvit, R., Hong, S. I., An, D. J., & Rhim, J. W. (2010). Effect of clay content on the physical and antimicrobial properties of whey protein isolate/organo-clay composite films. *LWT–Food Science and Technology, 43*(2), 279–284.

Srinivasa, P. C., Ramesh, M. N., & Tharanathan, R. N. (2007). Effect of plasticizers and fatty acids on mechanical and permeability characteristics of chitosan films. *Food Hydrocolloids, 21*(7), 1113–1122.

Su, J. F., Huang, Z., Zhao, Y. H., Yuan, X. Y., Wang, X. Y., & Li, M. (2010). Moisture sorption and water vapor permeability of soy protein isolate/poly(vinyl alcohol)/glycerol blend films. *Industrial Crops and Products, 31*(2), 266–276.

Tripathi, S., Mehrotra, G. K., & Dutta, P. K. (2010). Preparation and physicochemical evaluation of chitosan/poly(vinyl alcohol)/pectin ternary film for food-packaging applications. *Carbohydrate Polymers, 79*(3), 711–716.

Tunc, S., & Duman, O. (2010). Preparation and characterization of biodegradable methyl cellulose/montmorillonite nanocomposite films. *Applied Clay Science, 48*(3), 414–424.

Van Oss, C. (1995). Hydrophobicity of biosurfaces—origin, quantitative determination and interaction energies. *Colloids and Surfaces, B: Biointerfaces, 5*(3), 91–110.

Waliszewski, K. N., Aparicio, M. A., Bello, L. A., & Monroy, J. A. (2003). Changes of banana starch by chemical and physical modification. *Carbohydrate Polymers, 52*(3), 237–242.

Wang, S. F., Shen, L., Tong, Y. J., Chen, L., Phang, I. Y., Lim, P. Q., et al. (2005). Biopolymer chitosan/montmorillonite nanocomposites: Preparation and characterization. *Polymer Degradation and Stability, 90*(1), 123–131.

Zhong, Y., Song, X. Y., & Li, Y. F. (2011). Antimicrobial, physical and mechanical properties of kudzu starch-chitosan composite films as a function of acid solvent types. *Carbohydrate Polymers, 84*(1), 335–342.